IEEE Access
Multidisciplinary | Rapid Review | Open Access Journal

Received July 15, 2019, accepted July 23, 2019, date of publication July 26, 2019, date of current version August 12, 2019.

Digital Object Identifier 10.1109/ACCESS.2019.2931356

The Study on Fabrication and Characterization of $Al_{0.2}In_{0.8}Sb/InAs_{0.4}Sb_{0.6}$ Heterostructures by Molecular Beam Epitaxy

JING ZHANG[1,2], HONGLIANG LV[1], (Member, IEEE), YIFENG SONG[3], HAIQIAO NI[2], ZHICHUAN NIU[2], AND YUMING ZHANG[1], (Senior Member, IEEE)

[1]The State Key Discipline Laboratory of Wide Band Gap Semiconductor Technology, School of Microelectronics, Xidian University, Xi'an 710071, China
[2]State Key Laboratory for Superlattices and Microstructures, Institute of Semiconductors, Chinese Academy of Sciences, Beijing 100083, China
[3]School of Engineering, University of Glasgow, Glasgow G12 8LT, U.K.

Corresponding author: Hongliang Lv (hllv@mail.xidian.edu.cn)

This work was supported in part by the National Defense Advanced Research Project under Grant 315xxxxx301, in part by the National Defense Innovation Program under Grant 48xx4, in part by the 111 Project under Grant B12026, in part by the National Key Technologies Research and Development Program of China under Grant 2018YFA03xxx01, in part by the Scientific Instrument Developing Project of the Chinese Academy of Science under Grant YJKYYQ2017xxx2, and in part by the National Natural Science Foundation of China under Grant 6150xxx6.

ABSTRACT $Al_{0.2}In_{0.8}Sb/InAs_{0.4}Sb_{0.6}$ heterostructures have been successfully grown on GaAs substrate by molecular beam epitaxy (MBE). The influence of three different metamorphic buffer layers on the transport properties and crystal quality of the samples has been investigated, which shows the highest electron mobility of 28000 $cm^2/V{\cdot}s$ and the two-dimensional electron gas (2DEG) concentration of $9.29\times10^{11}cm^{-2}$ at 300 K are obtained in the sample with a $Al_{0.2}In_{0.8}Sb$ metamorphic buffer layer. This result is attributed to a decrease in both dislocations and interface roughness scattering for sample A3 with an $Al_{0.2}In_{0.8}Sb$ metamorphic buffer layer. Meanwhile, a series of samples were grown in order to systematically study the effects of channel layer width, spacer layer width, and Si δ-doping density on the transport properties in the $Al_{0.2}In_{0.8}Sb/InAs_{0.4}Sb_{0.6}$ modulation-doped heterostructures. The scattering mechanisms of interface roughness scattering, dislocations scattering, polar optical phonon scattering, remote impurity scattering, alloy scattering, and inter-subband scattering have been discussed to examine their effect on electron mobility and the 2DEG concentration. The results show that the highest electron mobility of 26500 $cm^2/V{\cdot}s$ and the 2DEG concentration of $1.15\times10^{12}cm^{-2}$ at 300 K can be achieved in the $Al_{0.2}In_{0.8}Sb/InAs_{0.4}Sb_{0.6}$ modulation-doped heterostructures with a 30-nm channel, a 6-nm spacer layer width, and a $9.0\times10^{-18}cm^{-3}$ Si δ-doped layer.

INDEX TERMS High electron mobility, transport properties, $Al_{0.2}In_{0.8}Sb/InAs_{0.4}Sb_{0.6}$ heterostructures.

I. INTRODUCTION

InAs material has attracted wide attention due to the unique band structure and excellent microelectronic properties of the InAs/AlSb heterostructures [1]. To pursue higher working speed and lower power consumption, the highest electron mobility in all III–V binary compounds of InSb has generated considerable interest for fabrication of high-speed devices [2]. At present, the epitaxy materials of these high-speed devices have to be grown on semi-insulating substrates for device isolation and high-frequency performance, however, there is no semi-insulating InSb substrates, which would have been ideal for lattice matching to InSb. Therefore, semi-insulating GaAs or InP substrates are generally chosen to grow high mobility materials; InP substrates are fragile and costly, thus GaAs substrates are the most common choice. Unfortunately, due to the large lattice mismatch (14.6%) between InSb and GaAs substrate, growth of high-quality InSb is very challenging. To minimize the problem of lattice strain and improve mobility, InAsSb ternary alloy is anticipated to be a substitution of InSb and InAs. Therefore, InAsSb material is expected to become a strong competitor as a channel material in the next generation of HEMT [3]–[6].

A lot of theoretical studies and simulations of the InAsSb based heterostructures has been done by many groups to optimize structural parameters and enhance the 2DEG concentration and electron mobility in the devices [7]–[9]. The electron effective mass and band gap of InAsSb are lower than InAs. Especially when the Sb component is 60%, InAsSb

The associate editor coordinating the review of this manuscript and approving it for publication was Farid Boussaid.

has the lowest electronic effective mass of III-V compound semiconductors, even lower than InSb, thus $Al_{0.2}In_{0.8}Sb/InAs_{0.4}Sb_{0.6}$ have very high electron mobility and saturated electron drift velocity. Based on theoretical studies of transport properties in InAsSb-based quantum well heterostructures, Zeng *et al.* [9] propose a material design for InAsSb quantum well with AlInSb barrier. For theoretical calculation, it is suggested that electron mobility as high as 35000 $cm^2/V{\cdot}s$ could be achieved in the $Al_{0.2}In_{0.8}Sb/InAs_{0.4}Sb_{0.6}$ heterostructures. However, the current experimental results are far lower than the simulation results due to interface mismatch and other problems in the growth process. Therefore, the experimental research on $Al_{0.2}In_{0.8}Sb/InAs_{0.4}Sb_{0.6}$ heterostructures is of great significance for the application of this structure in high-speed devices.

In this paper, the transport characteristics of $InAs_{0.4}Sb_{0.6}$ under different structure and growth parameters has been discussed, including metamorphic buffer layer, channel width, spacer width, doping concentration, etc. The evidence of superior transport properties of $Al_{0.2}In_{0.8}Sb/InAs_{0.4}Sb_{0.6}$ heterostructures for HEMT applications are obtained.

II. EXPERIMENTS

All samples were grown on semi-insulating GaAs (001) substrate using GEN-II solid-source MBE system. After the oxide desorption process, a 100 nm GaAs buffer layer and a 100 nm GaSb buffer layer were subsequently deposited in order to smooth out the surface. Then three different 1.5 μm metamorphic buffer layers were used to study the transport properties of $InAs_{0.4}Sb_{0.6}$ heterostructures. For sample A1, a 1.5 μm AlSb layer was directly deposited onto the GaSb buffer layer and it acts as a bottom barrier layer and buffer, as shown in Figure 1(a). For sample A2, a 1.45 μm AlSb layer was grown on the GaSb buffer and acts as a buffer layer, then a 50 nm $Al_{0.2}In_{0.8}Sb$ layer was grown on top of AlSb acting as a bottom barrier layer, as shown in Figure 1(b). For sample A3, a 1.5 μm $Al_{0.2}In_{0.8}Sb$ layer was directly deposited on the GaSb buffer acting as both bottom barrier layer and buffer, as shown in Figure 1(c). Then the channel, upper barrier layer and cap layer were deposited at 420 °C on top, details given in Figure 1. The As/In ratio and the Sb/In ratio of $InAs_{0.4}Sb_{0.6}$ was kept at 3 and 6, respectively.

A series of samples were grown in order to systematically study the effects of channel layer width, spacer layer width, and δ-doping density on the transport properties and crystal quality in the $Al_{0.2}In_{0.8}Sb/InAs_{0.4}Sb_{0.6}$ heterostructures. The schematic of $Al_{0.2}In_{0.8}Sb/InAs_{0.4}Sb_{0.6}$ modulation-doped heterostructure is shown in Figure 2, a 5∼10 nm $Al_{0.2}In_{0.8}Sb$ spacer layer, a $3.47\times10^{18}cm^{-3}$ ∼$1.45\times10^{19}cm^{-3}$ Si δ-doped layer were added to the sample A3.

III. RESULTS AND DISCUSSION

A. THE INFLUENCES OF METAMORPHIC BUFFER LAYER ON $Al_{0.2}In_{0.8}Sb/InAs_{0.4}Sb_{0.6}$ HETEROSTRUCTURES

Despite the excellent characteristics of InAsSb, the lack of high quality lattice-matched semi-insulating substrates severely limited the developments. Thus, the AlSb and $Al_{0.2}In_{0.8}Sb$ were used metamorphic buffer layer to reduce the mismatch between InAsSb and GaAs substrates. Figure 3(a), (b) and (c) shows the 10×10 μm^2 AFM images obtained from the three samples. The root means square (rms) roughness of sample A1 is 2.4 nm and Sb metal particles can be observed. It may be an excessive antimony flux during the AlSb buffer layer growth leads to the accumulation of Sb elements which intermixes into the subsequent growth layer, resulting in the formation of Sb metal particles on

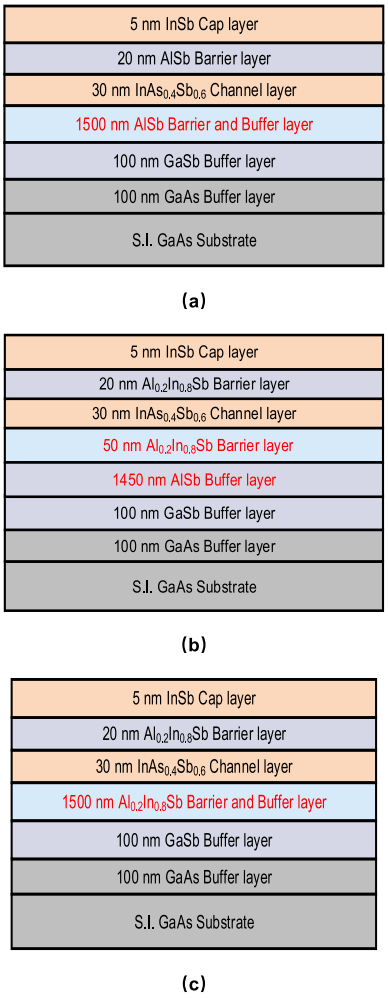

FIGURE 1. Schematic diagram of the structures of Al0.2In0.8Sb/InAs0.4Sb0.6 heterostructures. (a) Sample A1, (b) Sample A2 and (c) Sample A3.

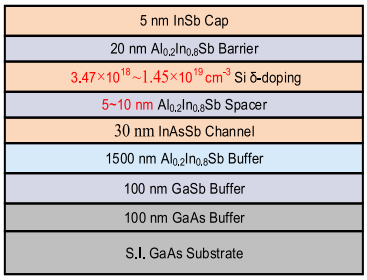

FIGURE 2. Schematic of $Al_{0.2}In_{0.8}Sb/InAs_{0.4}Sb_{0.6}$ modulation-doped heterostructures.

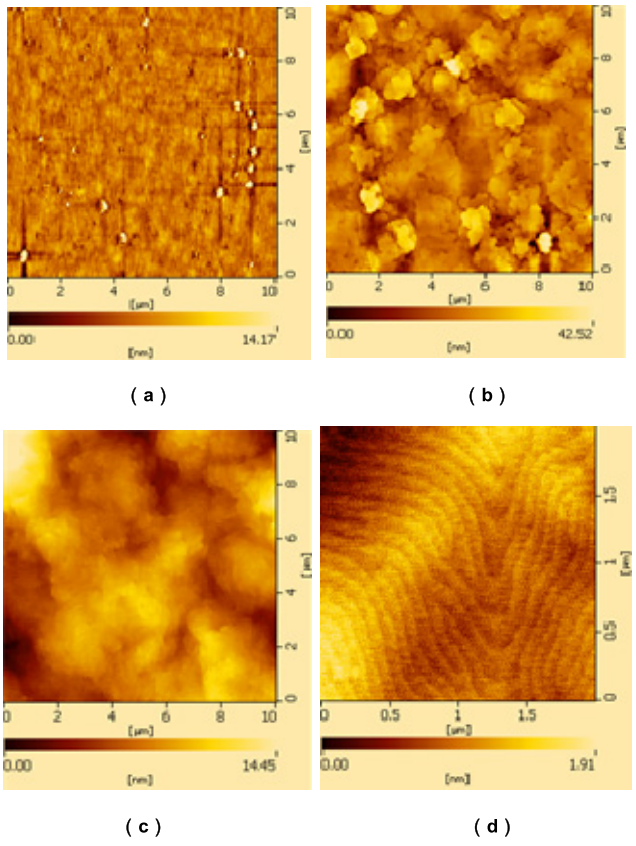

FIGURE 3. 10×10μm^2 AFM images of (a) Sample A1, (b) Sample A2 and (c) Sample A3; (d) 2×2μm^2 AFM images of Sample A3.

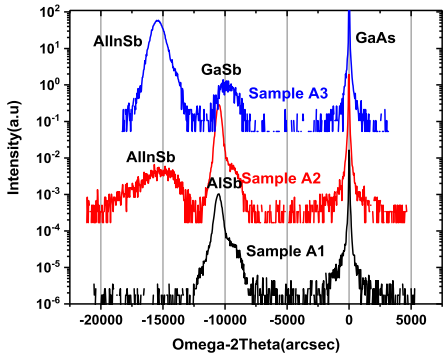

FIGURE 4. Double-crystal X-ray diffraction scans of (a) Sample A1, (b) Sample A2 and (c) Sample A3.

the surface of sample A1[4]. The surface of sample A2 is rough due to the 4.25% lattice mismatch between AlSb and $Al_{0.2}In_{0.8}Sb$ and its rms roughness is 5.3 nm. The sample A3 has the lowest rms roughness of 0.7 nm and the surface is relatively flat because $InAs_{0.4}Sb_{0.6}$ and $Al_{0.2}In_{0.8}Sb$ are lattice-matched. Figure 3(d) shows the 2×2 μm^{2}AFM image of sample A3. The atomic steps can be clearly seen, indicating that the surface of the sample A3 is very smooth.

The ω-2θ scan of symmetric (004) HRXRD spectra for all samples are shown in Figure 4. It can be seen from Figure 4 that the InAsSb channel layer was not observed for any of our samples due to the finite thickness. The (004) AlSb peak position is located at 30.1° and 30.11° for sample A1 and A2 respectively. In sample A3, the (004) $Al_{0.2}In_{0.8}Sb$ peak position is located at 28.75°. From the angle of peak position in (004) AlSb and (004) $Al_{0.2}In_{0.8}Sb$, the lattice constants can be determined to be 0.614 nm and 0.641 nm, respectively. It indicates that the strain of AlSb metamorphic buffer layer is 0.7% while that of $Al_{0.2}In_{0.8}Sb$ metamorphic buffer layer of sample A3 is almost completely relaxed.

To investigate the threading dislocations directly, the cross-sectional STEM micrographs of sample A1 and sample A3 are shown in Figure 5 (a) and (b), respectively. It can be seen from Figure 5 (a) and (b) that the white lines are the threading dislocation lines [10]. High density of threading dislocations in the sample A1 are generated at GaAs/GaSb/AlSb interfaces due to the large lattice mismatch. However, the $Al_{0.2}In_{0.8}Sb$ metamorphic buffer layer in the sample A3 filtrate the threading components very effectively, many of threading dislocations stopped at the $Al_{0.2}In_{0.8}Sb/InAs_{0.4}Sb_{0.6}$ interfaces. Interface flatness is also a key factor for controlling electron concentration and electron mobility in $InAs_{0.4}Sb_{0.6}$ based heterostructures. Figure 5 (c) and (d) show the cross-sectional TEM micrograph of $AlSb/InAs_{0.4}Sb_{0.6}$ heterostructures for sample A1 and $Al_{0.2}In_{0.8}Sb/InAs_{0.4}Sb_{0.6}$ heterostructures for sample A3. Flat interfaces between $Al_{0.2}In_{0.8}Sb$ and $InAs_{0.4}Sb_{0.6}$ layers are clearly seen for sample A3 due to the matched lattice constant.

Mobility is a crucial transport parameter used to evaluate the quality of $InAs_{0.4}Sb_{0.6}$ based heterostructures and to characterize the overall performance of high-speed devices. The electrical characterization of the various structures was examined by determining the Hall properties, as shown in Table 1. Hall measurements were performed on 1 cm×1 cm pieces at 300 K to obtain the electron mobility. The electron mobilities at 300K of sample A1, sample A2 and sample A3 are 7900 cm^2/V·s, 3700 cm^2/V·s and 28000 cm^2/V·s, respectively. Such a large difference in electron mobility is due to different scattering mechanisms. The major scattering mechanism in the $InAs_{0.4}Sb_{0.6}$ based heterostructures at 300 K are interface roughness scattering, polar optical phonon scattering, ionized impurity scattering, as well as acoustic phonon scattering and alloy scattering to a lesser extent [11]. Their relative contributions depending on temperature and structure parameters. Consequently, the relative importance of these types of scattering mechanisms may change accordingly. For example, the ionized impurity scattering includes remote ionized impurity scattering, background impurity scattering and dislocation scattering. For the different unintentionally doped $InAs_{0.4}Sb_{0.6}$ based heterostructures, the dislocation scattering plays a main role, while the remote ionized impurity scattering and background impurity scattering can be neglected [12]. Therefore, the electron mobility of sample A1, sample A2 and sample A3 at 300 K is determined by a combination of polar optical phonon scattering, interface roughness scattering and dislocation scattering. The component mobility of polar optical phonon scattering is

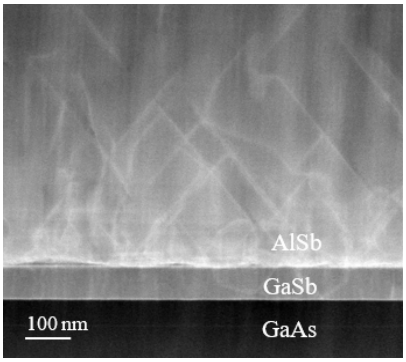

(a)

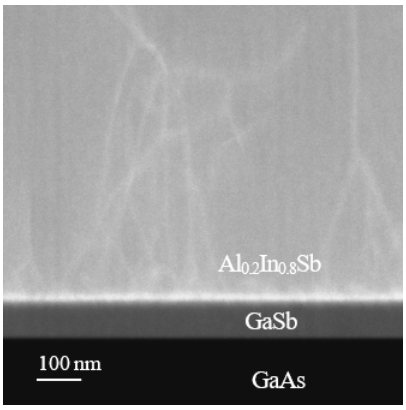

(b)

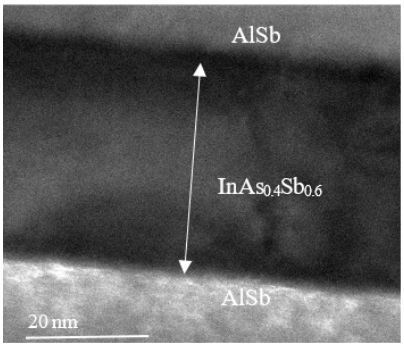

(c)

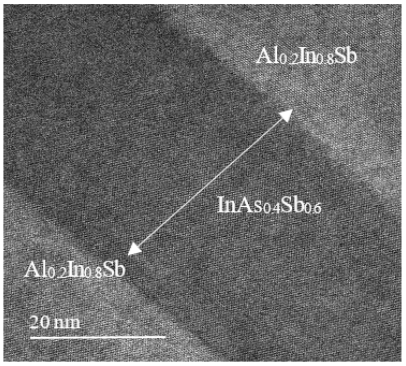

(d)

FIGURE 5. Cross-sectional STEM image of (a) the AlSb buffer structure for sample A1 and (b) the $Al_{0.2}In_{0.8}$ Sb buffer structure for sample A3; Cross-sectional TEM micrograph of (c) $AlSb/InAs_{0.4}Sb_{0.6}$ heterostructures for sample A1 and (d) $Al_{0.2}In_{0.8}Sb/InAs_{0.4}Sb_{0.6}$ heterostructures for sample A3.

TABLE 1. Hall measurements on the samples.

Sample	Electron mobility ($cm^2/V\cdot s$)	Sheet electron concentration (cm-2)
A1	7900	3.38×10^{12}
A2	3700	2.72×10^{12}
A3	28000	9.29×10^{11}

proportional to the dielectric constant of material [7]. For samples with the same InAsSb channel layer, polar optical phonon scattering is comparable therefore its contribution to the differences between the samples is much less than the other influences from dislocation scattering and interface roughness scattering. Corresponding to the analysis in Figure 5, the high density of threading dislocations and poor interface flatness can be clear seen in sample A1 due to the large lattice mismatch between AlSb and $InAs_{0.4}Sb_{0.6}$. A previous report by Egan *et al.* [13] shows that electron mobility is significantly affected by a high density of dislocations ($10^9 cm^{-2}$)in InAsSb based heterostructures; it also stated that record mobility can be reached by reducing the dislocation density to approximately $10^8 cm^{-2}$. Thus, the dislocation scattering and interface roughness scattering are the dominant mechanisms, which lead to a lower electron mobility in sample A1. In sample A2, the interface roughness scattering and dislocation scattering also affect the electron mobility in quantum wells due to the 4.25% lattice mismatch between AlSb and $Al_{0.2}In_{0.8}Sb$. Sample A3 has the highest mobility of 28000 $cm^2/V\cdot s$ due to the lower density of threading dislocations and flat interface. While alloy scattering is present in the $Al_{0.2}In_{0.8}Sb/InAs_{0.4}Sb_{0.6}$ structure, this effect does not offset the increase of mobility because of the tendency of high quality $InAs_{0.4}Sb_{0.6}$ channel layer towards narrower band gap and smaller effective mass [14].

B. THE INFLUENCES OF CHANNEL WIDTH ON $Al_{0.2}In_{0.8}Sb/InAs_{0.4}Sb_{0.6}$ HETEROSTRUCTURES

The influences of channel width on electron mobility was studied by using the unintentionally doped $Al_{0.2}In_{0.8}Sb/InAs_{0.4}Sb_{0.6}$ quantum wells, as shown in Figure 1(c). The thickness of $Al_{0.2}In_{0.8}Sb$ upper barrier layer and InSb cap layer were 20 nm and 5 nm, respectively, with the thickness of $InAs_{0.4}Sb_{0.6}$ channel varying from 15 to 45 nm. Figure 6 shows the electron mobility and 2DEG concentration dependence on channel width at 300 K. It can be observed that the electron mobility of samples increases quickly from 18500 cm^2/Vs to 28000 cm^2/Vs with the increase of the channel width from 15 nm to 30 nm. A similar situation was studied by Zeng et al. in InAs layer [15]. The interface roughness scattering is the main factor limiting the mobility in $InAs_{0.4}Sb_{0.6}$ channels thinner than 30 nm. Interface roughness which is exclusive in heterostructure systems originates from variation in the interfaces of the quantum well, this leads to spatial fluctuations and perturbation of electron confinement energy.

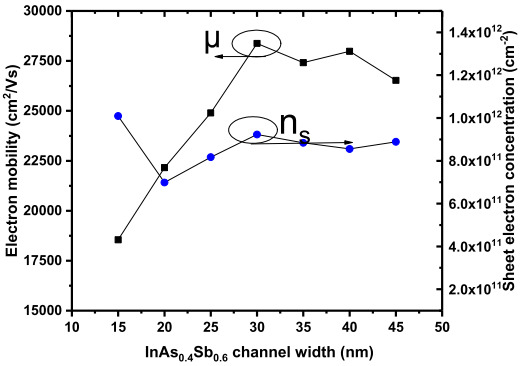

FIGURE 6. The electron mobility and 2DEG concentration versus channel width.

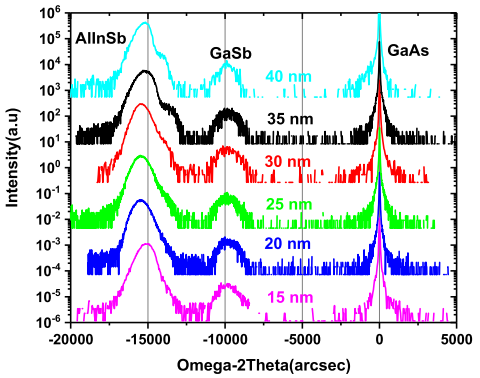

FIGURE 7. Double-crystal X-ray diffraction scans of (a) 15 nm, (b) 20 nm, (c)25 nm, (d) 30 nm, (e) 35 nm and (f) 40 nm.

This fluctuation and perturbation could generate local potential for electron scattering and is more significant in narrow quantum wells [11]. Additionally, a strong dependence on the channel width for this effect has been observed [16]. When the $InAs_{0.4}Sb_{0.6}$ channel width is 30 nm, the mobility reaches the maximum of 28000 cm^2/Vs. This phenomenon suggests that as the distribution of electrons gets farther away from the interfaces, electron confinement is improved [17], thereby weakening the interaction between electron wave function and scattering potential from interface roughness. When the channel width is larger than 30 nm, the electron mobility decreases slowly from 28000 cm^2/Vs to 26500 cm^2/Vs. It suggests that the interface roughness scattering decreases as the $InAs_{0.4}Sb_{0.6}$ channel width increases, but the stress in the $InAs_{0.4}Sb_{0.6}$ quantum well layer will be released in the form of threading dislocation. The electron mobility is dominated by dislocation scattering, polar optical phonon scattering and ionized impurity scattering [11]. Therefore, the electron mobility is no longer rising. For 2DEG concentration, a similar situation was studied by Chanh Nguyen et al. in the unintentionally doped InAs/AlSb quantum wells [12]. It can be seen from Figure 6 that large numbers of electrons as high as $6.99\times10^{11}cm^{-2}$ $\sim1.01\times10^{12}cm^{-2}$ that accumulate in the quantum well are attributed to the deep donor in the undoped $Al_{0.2}In_{0.8}Sb$ barrier layer, surface donors and the $Al_{0.2}In_{0.8}Sb/InAs_{0.4}Sb_{0.6}$ interface donor. With the thickness of the $InAs_{0.4}Sb_{0.6}$ channel layer increasing, there is a significant increase of 2DEG concentration, which indicates a gradual drain of electrons in the deep donor of the $Al_{0.2}In_{0.8}Sb$ barrier layer.

The ω-2θ scan of symmetric (004) XRD spectra for all samples are shown in Figure 7. Only three peaks can be seen in the Figure 7, which correspond to GaAs substrate, GaSb buffer layer and $Al_{0.2}In_{0.8}Sb$ metamorphic layer respectively. The $Al_{0.2}In_{0.8}Sb$ metamorphic layer of for all samples is clearly seen and has a full width at half maximum (FWHM) of 997 arcsec, 968 arcsec, 950 arcsec, 986 arcsec, 1108 arcsec and 914 arcsec, respectively. The similar FWHM and the position of the peak suggest that the $InAs_{0.4}Sb_{0.6}$ channel of all samples is coherently strained to the $Al_{0.2}In_{0.8}Sb$ barrier layer.

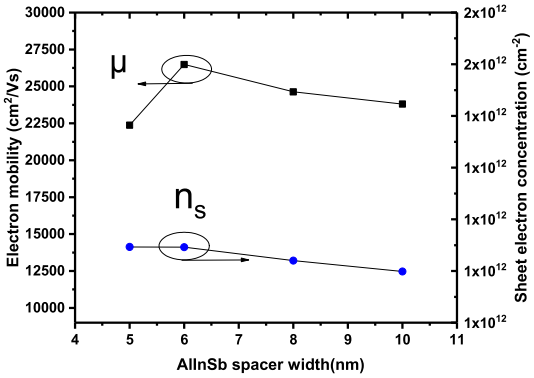

FIGURE 8. The electron mobility and 2DEG concentration versus spacer width.

C. THE INFLUENCES OF SPACER WIDTH ON $Al_{0.2}In_{0.8}Sb/InAs_{0.4}Sb_{0.6}$ MODULATION-DOPED HETEROSTRUCTURES

The structure of $Al_{0.2}In_{0.8}Sb$/ $InAs_{0.4}Sb_{0.6}$modulation-doped heterostructures is shown in Figure 2. A $9.0\times10^{18}cm^{-3}$ Si δ-doped layer in the $Al_{0.2}In_{0.8}Sb$ upper barrier layer and the thickness of $InAs_{0.4}Sb_{0.6}$ channel layer, $Al_{0.2}In_{0.8}Sb$ upper barrier layer and InSb cap layer were 30 nm, 20 nm, 5 nm, respectively. The thickness of $Al_{0.2}In_{0.8}Sb$ spacer layer vary from 5 to 10 nm. Figure 8 shows the electron mobility and 2DEG concentration dependence on spacer width at 300 K. As the thickness of $Al_{0.2}In_{0.8}Sb$ spacer layer decreases from 10 to 5 nm, there are two competing processes which will affect the electron mobility. On the one hand, in the case for decreasing the spacer width from 10 nm to 6 nm, more electrons transfer into the quantum well resulting in improved 2DEG concentrations from 1.09×10^{12} cm^{-2} to 1.15×10^{12} cm^{-2}. The remote ionized impurity scattering will be effectively screened by 2DEG concentration in quantum wells, leading to the electron mobility increasing from 23800 cm^2/V·s to 26500 cm^2/V·s. On the other hand, in the case for decreasing the spacer width from 6 nm to 5 nm, the distance between ionized impurities and quantum wells decreases, the remote ionized impurity scattering increases and the electron mobility decreases accordingly.

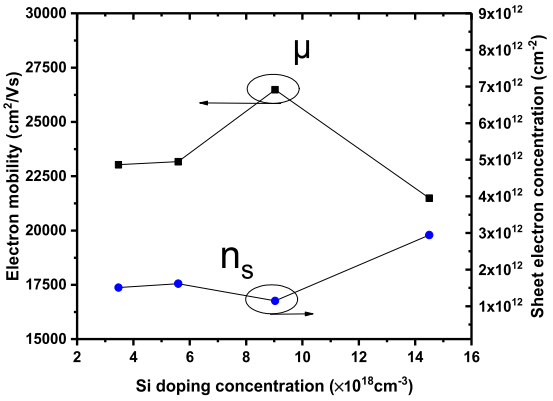

FIGURE 9. The electron mobility and 2DEG concentration versus Si δ-doping density.

Therefore, the above two factors should be taken into account when choosing the thickness of $Al_{0.2}In_{0.8}Sb$ spacer layer. The highest electron mobility of $Al_{0.2}In_{0.8}Sb/InAs_{0.4}Sb_{0.6}$ modulation-doped heterostructures with a 6 nm $Al_{0.2}In_{0.8}Sb$ spacer layer is 26500 $cm^2/V{\cdot}s$.

D. THE INFLUENCE OF δ -DOPING DENSITY ON $Al_{0.2}In_{0.8}Sb/InAs_{0.4}Sb_{0.6}$ MODULATION-DOPED HETEROSTRUCTURES

The structure of Figure 2 is also used to study the influence of δ-doping density on $Al_{0.2}In_{0.8}Sb/InAs_{0.4}Sb_{0.6}$ modulation-doped heterostructures. The range of Si doping investigated (in the Si δ-doped layer) is $3.47\times10^{18}cm^{-3}$ $\sim1.45\times10^{19}cm^{-3}$.

As shown in Figure 9, when the remote doping concentration is less than $9.0\times10^{-18}cm^{-3}$, the electron mobility increases to 26500 $cm^2/V{\cdot}s$ with the increase of doping concentration. In this range, only the first subband is occupied by electrons, 2DEG concentration correspondingly enhances the screened effect on scattering, and the electron mobility shows an upward trend. To further increase the remote doping concentrations to $1.45\times10^{-19}cm^{-3}$, the second subband energy has dropped below the Fermi energy level and enough electrons have occupied it. At which point inter-subband scattering turns on and an abrupt lowering to 21500 $cm^2/V{\cdot}s$ in the electron mobility is observed [18]. In addition, at 300K, optical phonon scattering has a more significant effect on electrons at high energy levels [19]. Moreover, with the increase of remote doping concentrations, the subband energy levels goes deep into the bottom of the quantum well and the electron wave function is closer to the interface [20], [21]. Therefore, the sharp decrease of electron mobility can be partly explained by enhanced interface roughness scattering and optical phonon scattering.

IV. CONCLUSION

In conclusion, the influence of three different metamorphic buffer layers on the transport properties and crystal quality of the $Al_{0.2}In_{0.8}Sb/InAs_{0.4}Sb_{0.6}$ heterostructures has been investigated, which shows the highest electron mobility due to a decrease in both dislocations and interface roughness scattering. The variation in the channel width, spacer layer width and δ-doping density have significant effect on the 2DEG concentration and electron mobility, a 30 nm channel, a 6 nm spacer layer width and a $9.0\times10^{-18}cm^{-3}$ Si δ-doped layer is the optimized parameters for the $Al_{0.2}In_{0.8}Sb/InAs_{0.4}Sb_{0.6}$ modulation-doped heterostructures. Room temperature electron mobility of 26500 $cm^2/V{\cdot}s$ and 2DEG concentration of $1.15\times10^{12}cm^{-2}$ have been achieved in the optimized sample. This is comparable with previous attempts to grow the $InAs_{0.2}Sb_{0.8}$ channel layer using a digital alloy procedure [22]. The scattering mechanisms of interface roughness scattering, dislocations scattering, polar optical phonon scattering, remote impurity scattering, alloy scattering and inter-subband scattering have been discussed to examine their effect on electron mobility and 2DEG concentration. The superior transport properties of $Al_{0.2}In_{0.8}Sb/InAs_{0.4}Sb_{0.6}$ heterostructures for HEMT applications are obtained.

REFERENCES

[1] G. Moschetti, E. Lefebvre, M. Fagerlind, P. Å. Nilsson, L. Desplanque, X. Wallart, and J. Grahn, "DC, RF and noise performance of InAs/AlSb HEMTs with *in situ* CVD SiN_x-film for early-protection against oxidation," *Solid-State Electron.*, vol. 87, pp. 85–89, Sep. 2013.

[2] M. Edirisooriya, T. D. Mishima, C. K. Gaspe, K. Bottoms, R. J. Hauenstein, and M. B. Santos, "InSb quantum-well structures for electronic device applications," *J. Crystal Growth*, vol. 311, no. 7, pp. 1972–1975, Mar. 2009.

[3] C. Liao and K. Y. Cheng, "The growth of high electron mobility InAsSb for application to high electron-mobility transistors," *J. Crystal Growth*, vol. 311, no. 7, pp. 1976–1978, Mar. 2009.

[4] B. P. Tinkham, B. R. Bennett, R. Magno, B. V. Shanabrook, and J. B. Boos, "Growth of InAsSb-channel high electron mobility transistor structures," *J. Vac. Sci. Technol. B, Microelectron.* vol. 23, no. 4, pp. 1441–1444, Jul. 2005.

[5] Y. Zhang, Y. Zhang, M. Guan, L. Cui, Y. Li, B. Wanga, Z. Zhu, and Y. Zeng, "Molecular beam epitaxial growth of AlSb/InAsSb heterostructures," *Appl. Surf. Sci.*, vol. 313, pp. 479–483, Sep. 2014.

[6] C. Liao, B.-R. Wu, K. C. Hsieh, and K. Y. Cheng, "High electron mobility $InAs_{0.8}Sb_{0.2}$ grown on InP substrates by gas source molecular beam epitaxy," *J. Vac. Sci. Technol. B, Microelectron.*, vol. 26, no.3, pp. 1078–1080, May 2008.

[7] Y. Zhang, Y. Zhang, C. Wang, and Y. Zeng, "Transport properties in AlInSb/InAsSb heterostructures," *J. Appl. Phys.*, vol. 114, no. 24, Dec. 2013, Art. no. 243710.

[8] G. Devakadaksham, M. Kumar, and C. K. Sarkar, "Threading dislocation degradation of InSb to InAsSb subchannel double heterostructures," *Electron. Mater. Lett.*, vol. 11, no. 4, pp. 580–585, Jul. 2015.

[9] Y. Zhang, Y. Zhang, C. Wang, and Y. Zeng, "Transport properties in AlInSb/InAsSb heterostructures," *J. Appl. Phys.*, vol. 114, no. 24, Dec. 2013, Art. no. 243710.

[10] Y. Shi, D. Gosselink, K. Gharavi, J. Baugh, and Z. R. Wasilewski, "Optimization of metamorphic buffers for MBE growth of high quality AlInSb/InSb quantum structures: Suppression of hillock formation," *J. Crystal Growth*, vol. 477, pp. 7–11, Nov. 2017.

[11] Y. Zhang, Y. Zhang, M. Guan, L. Cui, C. Wang, and Y. Zeng, "Theoretical study of transport property in InAsSb quantum well heterostructures," *J. Appl. Phys.*, vol. 114, no. 15, Oct. 2013, Art. no. 153707.

[12] C. Nguyen, B. Brar, J. English, and H. Kroemer, "Effects of barrier thicknesses on the electron concentration in not-intentionally doped InAs–AlSb quantum wells," *J. Vac. Sci. Technol. B, Microelectron.*, vol. 10, no. 2, pp. 898–900, Mar. 1992.

[13] R. J. Egan, V. W. L. Chin, and T. L. Tansley, "Dislocation scattering effects on electron mobility in InAsSb," *J. Appl. Phys.*, vol. 75, no. 5, pp. 2473–2476, Mar. 1994.

[14] M. Y. Yen, B. F. Levine, C. G. Bethea, K. K. Choi, and A. Y. Cho, "Molecular beam epitaxial growth and optical properties of $InAs_{1-x}Sb_x$ in 8–12 μm wavelength range," *Appl. Phys. Lett.*, vol. 50, no. 14, pp. 927–929, Apr. 1987.
[15] Z. Yang, Z. Yu-Wei, W. Cheng-Yan, G. Min, C. Li-Jie, L. Yi-Yang, W. Bao-Qiang, Z. Zhan-Ping, and Z. Yi-Ping, "High sensitivity Hall devices with AlSb/InAs quantum well structures," *Chin. Phys. B*, vol. 22, no. 5, May 2013, Art. no. 057106.
[16] A. Gold, "Interface-roughness parameters in InAs quantum wells determined from mobility," *J. Appl. Phys.*, vol. 103, no. 4, Feb. 2008, Art. no. 043718.
[17] L. Hsu and W. Walukiewicz, "Electron mobility in $Al_xGa_{1-x}N$/GaN heterostructures," *Phys. Rev. B, Condens. Matter*, vol. 56, no. 3, pp. 1520–1528, Jul. 1997.
[18] T. Sahu and J. Patnaik, "Electron transport mobility in a δ-doped double quantum well structure," *J. Appl. Phys.*, vol. 88, no. 5, pp. 2658–2664, Sep. 2000.
[19] B. Gelmont, K. Kim, and M. Shur, "Monte Carlo simulation of electron transport in gallium nitride," *J. Appl. Phys.*, vol. 74, no. 3, pp. 1818–1821, Aug. 1993.
[20] I. P. Smorchkova, C. R. Elsass, J. P. Ibbetson, R. Vetury, B. Heying, P. Fini, E. Haus, S. P. DenBaars, J. S. Speck, and U. K. Mishra, "Polarization-induced charge and electron mobility in AlGaN/GaN heterostructures grown by plasma-assisted molecular-beam epitaxy," *J. Appl. Phys.*, vol. 86, no. 8, p. 4520, 1999.
[21] J. Antoszewski, M. Gracey, J. M. Dell, L. Faraone, T. A. Fisher, G. Parish, Y.-F. Wu, and U. K. Mishra, "Scattering mechanisms limiting two-dimensional electron gas mobility in $Al_{0.25}Ga_{0.75}N$/GaN modulation-doped field-effect transistors," *J. Appl. Phys.*, vol. 87, no. 8, pp. 3900–3904, Apr. 2000.
[22] M. Kudo, T. Mishima, and T. Tanaka, "Increased electron mobility of InAsSb channel heterostructures grown on GaAs substrates by molecular beam epitaxy," *J. Vac. Sci. Technol. B, Microelectron.*, vol. 18, no. 2, pp. 746–750, Mar. 2000.

JING ZHANG received the M.S. degree from the School of Telecommunications, Shaanxi University of Science and Technology, Xi'an, China, in 2013. She is currently pursuing the joint Ph.D. degree with the School of Microelectronics, Xidian University, and with the Institute of Semiconductors, Chinese Academy of Sciences. Her current research interests include the growth of III–V material and fabrication of the high electron mobility transistors (HEMTs).

HONGLIANG LV was born in Tulufan, China, in 1978. She received the M.S. and Ph.D. degrees in microelectronics engineering from Xidian University, Xi'an, China, in 2003 and 2007, respectively, where she has been a Professor with the School of Microelectronics, since 2010. Her work involves the modeling and experiments on SiC MESFET and other devices.

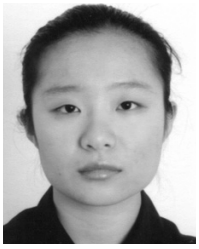

YIFENG SONG received the B.Sc. and M.Sc. degrees in natural sciences from the University of Cambridge, U.K., in 2014. She is currently pursuing the Ph.D. degree with the University of Glasgow. Her current research interest includes the integration of membrane III–V devices onto silicon photonic chips.

HAIQIAO NI received the Ph.D. degree from the National University of Singapore. He is currently a Researcher with the State Key Laboratory for Superlattices and Microstructures, Institute of Semiconductors, Chinese Academy of Sciences. His research interests include the growth and physical analysis of III-V semiconductor materials.

ZHICHUAN NIU received the Ph.D. degree from the Institute of Semiconductors, Chinese Academy of Sciences, where he is currently a Researcher with the State Key Laboratory for Superlattices and Microstructures. His research interests include the growth of molecular beam epitaxy of low dimensional III–V semiconductor materials, the quantum effect of limited optoelectronic system, and the preparation of high performance optoelectronic quantum devices.

YUMING ZHANG received the M.S. degree from Xidian university, Xi'an, China, in 1992, and the Ph.D. degree from Xi'an Jiaotong University, Xi'an, in 1998. Since 2001, he has been a Professor with the Microelectronics Institute, Xidian University. His research interests include the design, modeling, fabrication, and electrical characterization of SiC electronic devices for high-temperature and high-power operation.